JGR Atmospheres

RESEARCH ARTICLE
10.1029/2024JD043047

Moisture Source Controls on Water Isotopes in Antarctic Precipitation—Insights From Water Tracers in ECHAM6-Wiso

Qinggang Gao[1,2,3], Louise C. Sime[1], Alison J. McLaren[1], and Martin Werner[4]

[1]Ice Dynamics and Paleoclimate, British Antarctic Survey, Cambridge, UK, [2]Department of Earth Sciences, University of Cambridge, Cambridge, UK, [3]Now at School of Geography, Earth and Atmospheric Sciences, University of Melbourne, Parkville, VIC, Australia, [4]Helmholtz Centre for Polar and Marine Research, Alfred Wegener Institute, Bremerhaven, Germany

Key Points:

- The deuterium excess of Antarctic precipitation primarily reflects moisture source sea surface temperature (SST), making it a strong proxy for past SST in ice cores
- The logarithmic definition of deuterium excess better captures the influences of moisture sources than the traditional linear definition
- Deuterium excess is more sensitive to source SST farther inland, and their relationship is strongly modulated along moisture transport

Correspondence to:
Q. Gao,
qinggang.gao@unimelb.edu.au

Citation:
Gao, Q., Sime, L. C., McLaren, A. J., & Werner, M. (2025). Moisture source controls on water isotopes in Antarctic precipitation—Insights from water tracers in ECHAM6-wiso. *Journal of Geophysical Research: Atmospheres*, *130*, e2024JD043047. https://doi.org/10.1029/2024JD043047

Received 3 DEC 2024
Accepted 5 JUL 2025

Abstract The interpretation of water isotope records in Antarctic ice cores is crucial for our understanding of past climate changes. Here we use novel water tracers in an ECHAM6-wiso simulation to investigate moisture source controls on deuterium excess in Antarctic precipitation, particularly the logarithmic variant d_{ln}. The simulation captures the amplitude of seasonal changes in observed δD and d_{ln} of precipitation. There are, however, some model biases that cannot be resolved through adjustments to kinetic fractionation parameters or the model resolution. These may reflect issues in the hydrological cycle representation or the representation of isotope processes. The simulated d_{ln} in Antarctic precipitation reliably reflects moisture source sea surface temperature (SST): d_{ln} shows a higher correlation than traditionally defined deuterium excess. Ocean surface relative humidity with respect to SST (RHsst) influences d_{ln} during evaporation, however, this influence weakens above the ocean surface. 79% of the variance in d_{ln} of annual precipitation at Dome C is due to changes in moisture source SST. d_{ln} is more sensitive to source SST in inland Antarctica than in coastal regions, making it a robust proxy for reconstructing past SST at the inland ice core sites. The explained variance of d_{ln} by source SST for daily precipitation at Dome C is lower at 28%, which increases to 59% after excluding very low precipitation days (<0.02 mm). Finally, we find reversed relationships between source SST and d_{ln} in the vapor above the Southern Ocean, potentially driven by cold air outbreaks or precipitation processes.

Plain Language Summary The heavy-to-light isotope ratios of atmospheric water capture a range of hydrological processes, making them a vital tool for studying the water cycle. Decades ago, scientists discovered an empirical relationship between isotope ratios in Antarctic surface snow and local surface temperature, which has since been used to infer past temperatures from Antarctic ice cores. Recent modeling studies, with an improved understanding of water isotope fractionation, have expanded this approach to also extract moisture source information from ice core records. However, interpreting moisture source properties from water isotopes has remained uncertain. In this study, we use new advanced modeling tools that provide precise information about moisture sources to directly assess what water isotopes reveal about these properties. These findings offer new insights into the hydrological cycle and enhance our ability to analyze isotope records.

1. Introduction

Antarctic climate is rapidly changing, with record low sea ice extent and extreme heat events in 2022 and 2023 (Diamond et al., 2024; Gorodetskaya et al., 2023; Purich & Doddridge, 2023). Increased moisture in the region directly drives warming, as model simulations show that poleward moisture transport is a key contributor to the future Antarctic warming (Hahn et al., 2021). Warming Southern Ocean waters may accelerate sea ice and ice shelf loss, altering evaporation patterns and impacting Antarctic precipitation and surface mass balance (Mottram et al., 2021). These changes could affect the Antarctic mass budget and contribute to future sea level rise, although the extent remains uncertain (IPCC, 2021). Understanding evaporative source changes is critical for predicting these impacts, but tracking these changes (e.g., Fiorella et al., 2021; Sodemann & Stohl, 2009; Werner et al., 2001), both in the present and past, has been challenging.

Going further back in time, ice cores provide information on climate changes over hundreds of thousands of years (EPICA community members, 2004). Water isotopes from ice cores have long served as proxies for past temperature changes, especially during glacial-interglacial cycles (Jouzel et al., 2007). These reconstructions rely on

quasi-linear relationships between isotope ratios in surface snow and local surface temperature (Jouzel et al., 2003), but shifts in moisture sources can introduce uncertainties (Landais et al., 2021; Stenni et al., 2010). More information about Antarctic precipitation and moisture sources could improve our understanding of current, future, and past Antarctic climate and the drivers of ice mass budget changes. It could also be essential for understanding the impacts of anthropogenic climate change and potential tipping points in the Earth system (Casado et al., 2023; Lenton et al., 2019).

Given these needs, moisture source information has been inferred from water isotopes, which are stable isotopologues of hydrogen and oxygen, including H_2O, $H_2^{18}O$, and HDO. These isotopologues are measured relative to a standard due to the rare abundance of the heavier isotopologues. The isotope ratios are expressed as $\delta = (R_{sample} - R_{V\ SMOW})/R_{V\ SMOW} \times 1000$ [‰], where R_{sample} and $R_{V\ SMOW}$ represent the ratios of D/H or $^{18}O/^{16}O$ in the sample and in Vienna Standard Mean Ocean Water (VSMOW), respectively (Jouzel, 2014). Fractionation of these water isotopes occurs during phase changes, driven by differences in saturation vapor pressures and molecular diffusivities. This fractionation can be either equilibrium or kinetic. Equilibrium fractionation is governed by temperature-dependent fractionation factors α, which define the isotope ratios between two phases (Majoube, 1971b). Kinetic fractionation, on the other hand, results in a relative enrichment of HDO compared to $H_2^{18}O$ in the less strongly bound phase, due to the higher molecular diffusivity of HDO (Merlivat, 1978; Pfahl & Sodemann, 2014). Kinetic fractionation can occur during ocean surface evaporation, snow formation in mixed clouds, and precipitation re-evaporation (Jouzel & Merlivat, 1984; Merlivat & Jouzel, 1979; Risi et al., 2008). Of these, the kinetic fractionation that occurs during ocean surface evaporation is of particular interest: this imprints ocean surface properties, particularly SST and RHsst, in the evaporated vapor isotope ratios (Jouzel et al., 1982; Landais et al., 2021).

To help quantify these kinetic fractionation processes, Dansgaard (1964) introduced a linear definition of deuterium excess, $d_{xs} = \delta D - 8\delta^{18}O$, based on the global meteoric water line (Craig, 1961). However, since d_{xs} is influenced by the nonlinearity of the δ scale (as $\ln(1 + \delta) \neq \delta$), Uemura et al. (2012) proposed a logarithmic definition of deuterium excess: $d_{\ln} = \ln(1 + \delta D) - 8.47 \times \ln\left(1 + \delta^{18}O\right) + 28.5 \times \left(\ln\left(1 + \delta^{18}O\right)\right)^2$. Deuterium excess ($d_{xs}$ and $d_{\ln}$) in ocean surface evaporative fluxes is positively correlated with SST and negatively correlated with RHsst when other conditions remain constant (Hoffmann et al., 1998, see their Eq. 2).

Factors that influence deuterium excess have been explored using observation data sets (e.g., Benetti et al., 2014; Uemura et al., 2008; Pfahl & Wernli, 2008). For example, based on 2 years of vapor isotope observations on a cruise from the Arctic to the Southern Ocean, a spatial relationship, $d_{xs} = -0.33RHsst + 0.27SST + 25.01$, was established for 6-hourly data (Bonne et al., 2019). However, cross correlations between SST and RHsst may complicate their relationships with deuterium excess (Aemisegger & Sjolte, 2018). Specifically, Aemisegger (2018) found that strong large-scale ocean evaporation in the subpolar North Atlantic induced by cold advection in the rear of extratropical cyclones could result in positive anomalies of deuterium excess and negative anomalies of SST, thus reversed relationships between deuterium excess and source SST. Similar negative temporal correlations between deuterium excess and source SST have also been found in the study of Pfahl and Wernli (2008) and Sodemann et al. (2024), which contradict results from spatial relationships between deuterium excess and source SST (Bonne et al., 2019). Furthermore, these correlations can also be altered by additional processes during the transport of moisture in the atmosphere, which can result in different deuterium excess relationships in precipitation and vapor fields. Generally, these studies indicate that deuterium excess in ocean surface vapor contains information on evaporative conditions, specifically on RHsst and SST, although possibly not on wind speed. It is not clear from these studies whether this information is preserved in Antarctic precipitation.

Links between deuterium excess and moisture sources, and implications of using d_{xs} or $d_{\ln}$, have also been explored using simple water-isotope distillation models (Ciais & Jouzel, 1994). Merlivat and Jouzel (1979) evaluated the controls of moisture sources on deuterium excess, assuming a steady-state regime where the isotope compositions of global precipitation are equal to those of evaporation and vapor. They found that δD and $\delta^{18}O$ are linearly related, with both slope and intercept controlled by moisture source SST and RHsst. The application of d_{xs}, however, involves an artifact due to the approximation $\ln(1 + \delta) = \delta$ (Uemura et al., 2012), which leads to a higher d_{xs} in depleted water vapor (Dütsch et al., 2017). Although this artifact can be avoided by using $d_{\ln}$, $d_{\ln}$ is not conserved during the mixing of air parcels due to its logarithmic definition. However, Dütsch et al. (2017)

found that this mixing effect is negligible for small differences in isotope ratios between air parcels (e.g., ±8‰ in δD), but stronger effects may occur for air parcels with distinct isotope compositions. Although Jouzel and Merlivat (1984) showed that kinetic fractionation during snow formation can influence deuterium excess, Markle and Steig (2022) argued that nonlinearities in the water-isotope-temperature relationships further complicate the interpretation of water isotopes under different meteorological conditions. In summary, studies using simple distillation models do not make it very clear whether the use of d_{xs} or $d_{\ln}$ is more accurate when inferring moisture source properties.

Atmospheric models that simulate the entire hydrological cycle, and which are equipped with water isotope capabilities, are perhaps the most comprehensive means to investigate evaporative source controls on deuterium excess (Jouzel et al., 2013). For example, Risi et al. (2013) used the general circulation model (GCM) LMDZ to investigate the factors that control the spatio-temporal distribution of precipitation d_{xs}. They found that seasonal variations of d_{xs} at high latitudes are mainly affected by evaporative conditions, Rayleigh distillation, and supersaturation during condensation at low temperatures. Fiorella et al. (2021) then developed new process-orientated tracers which were used to examine the controls of moisture sources on deuterium excess in the water isotope enabled GCM iCAM6. These types of tracers provide a new means to more accurately diagnose the source properties of Antarctic precipitation (Gao et al., 2024). For example, in a preindustrial simulation using ECHAM6-wiso, Gao et al. (2024) found that annual mean Antarctic precipitation originating from the open ocean has a source latitude range of 49–35°S and a source SST range of 10–16°C.

Building directly on these recent model developments, here we use newly developed water tracers in ECHAM6-wiso to examine moisture source controls on water isotopes in Antarctic precipitation (Gao et al., 2024). Modeled relationships between moisture source properties and the two definitions (d_{xs} and $d_{\ln}$) of deuterium excess in precipitation and vapor are examined at daily, monthly, and annual timescales. We focus primarily on Dome C, where the oldest ice core was extracted (EPICA community members, 2004) and a million-year-old ice core is being drilled nearby (Chung et al., 2023) but also look more broadly across another Antarctic station and the Antarctic region. Section 2 presents the model, present day observation of water isotopes from the Antarctic region and methods. Section 3.1 contains an evaluation of the model simulations against these observations. Section 3.2 presents analysis of source evaporative controls on deuterium excess in precipitation and vapor. Section 4 provides conclusions and some discussion of the implications of the results.

2. Data and Methods

2.1. ERA5-Nudged ECHAM6-Wiso Simulations

The ECHAM6 model was developed by the Max Planck Institute for Meteorology (Stevens et al., 2013). ECHAM6 consists of a spectral-transform dynamical core, physical parameterizations for diabatic processes, a transport model for scalar quantities other than temperature and surface pressure, and boundary data sets for externalized parameters.

The water isotope module of ECHAM6-wiso is presented in Cauquoin et al. (2019). The equilibrium fractionation coefficients between the vapor and liquid/ice water are derived from Merlivat and Nief (1967) and Majoube (1971a, 1971b). Based on observations of Bonne et al. (2019), Cauquoin and Werner (2021) set the kinetic fractionation coefficient for $\delta^{18}O$ during ocean surface evaporation as a constant $k_{18} = 0.00475$, which is independent of wind speed as opposed to Merlivat and Jouzel (1979). Using Antarctic snow isotope measurements from Masson-Delmotte et al. (2008), Cauquoin and Werner (2021) parameterize the supersaturation condition during snow formation (Jouzel & Merlivat, 1984) as $S = 1.02 - 0.0045T$, where T is the condensation temperature in °C. The isotope fractionation during raindrop reevaporation is parameterized after Hoffmann et al. (1998), where the isotope equilibrium with the surrounding vapor is reached to 45% in convective precipitation with large raindrops and to 95% in large-scale precipitation with small raindrops.

Following up the latest development of water tracers in Fiorella et al. (2021), Gao et al. (2024) employed and further developed their approach to quantify moisture source locations and properties of atmospheric humidity and precipitation in ECHAM6-wiso. Building upon the model code infrastructure of water isotopes, scaled-flux water tracers were implemented to infer the mass-weighted mean open-ocean evaporative source locations and properties of moisture. These source properties include the mass-weighted mean open-ocean evaporative source latitude (source latitude hereafter), longitude, SST, 2 m relative humidity (rh2m), and 10 m wind velocity (vel10).

Table 1
Sensitivity Experiments of Kinetic-Fractionation-Related Parameters Using ECHAM6-Wiso

Experiments	Kinetic fractionation coefficient for $\delta^{18}O$ [−]	Intercept of supersaturation function [−]	Slope of supersaturation function [$°C^{-1}$]
control	0.00475	1.02	0.0045
k52	**0.0052**	1.02	0.0045
k43	**0.0043**	1.02	0.0045
I01	0.00475	**1.01**	0.0045
I03	0.00475	**1.03**	0.0045
S3	0.00475	1.02	**0.003**
S6	0.00475	1.02	**0.006**

Note. Changed parameters are indicated in bold.

In addition to the evaporative properties tracked in Gao et al. (2024), we also trace the evaporative RHsst, which is defined as

$$RHsst = \frac{q}{q_s}, \tag{1}$$

where q denotes specific humidity at the lowest model level, and q_s saturation specific humidity at SST.

Our ECHAM6-wiso simulations are rerun from a 30-year spin-up simulation of Cauquoin and Werner (2021), for which they use fixed boundary conditions of 1979. Our water tracer simulations are then spun up for five model years in the same manner. We follow the approach of Cauquoin and Werner (2021) to nudge the 3D temperature, vorticity, divergence, and surface pressure of the simulations to the ERA5 reanalysis (Hersbach et al., 2020). The monthly SST and sea ice concentration as given by the ERA5 reanalysis, as well as a global gridded data set of annual mean $\delta^{18}O$ of surface seawater (LeGrande & Schmidt, 2006), are provided as boundary conditions of the ocean surface. As there is no equivalent data set for δD of seawater, δD of surface seawater is assumed to be eight times of $\delta^{18}O$ of seawater (Cauquoin & Werner, 2021). The simulations are run for 44 years from 1979 to 2022 at a horizontal resolution of 1.87° × 1.87° with 47 vertical levels extending to 0.01 hPa.

In addition to the *control* simulation, six sensitivity experiments are carried out by varying three parameters related to kinetic fractionation and supersaturation in reasonable ranges (Table 1). Setting the kinetic fractionation coefficient for $\delta^{18}O$ as $k_{18} = 0.0052$ in the *k52* simulation follows results of Zannoni et al. (2022).

For data analysis, daily model output is used. We use nearest-neighbor interpolation to extract the model output for an observation site. The surface specific humidity and its isotope compositions from model simulations are extracted from the lowest model level, around 30 m above the surface.

2.2. Observations of Water Isotopes

Measurements of water isotopes in precipitation and surface vapor are presented here, and used to evaluate model performance. Although the main focus is on the Dome C site, surface vapor isotopes at Kohnen station and over the ocean are also used to explore model-data discrepancies. All water isotope ratios are weighted by mass (precipitation or specific humidity).

2.2.1. Precipitation Isotopes at Dome C

Stenni et al. (2016) measured daily precipitation amounts and isotope compositions for three years (2008–2010) at Concordia station. Concordia station is located at Dome C in East Antarctica (75°06′S, 123°21′ E, 3,233 m above sea level, Figure A1). Depending on the precipitation sample amount, the isotope compositions were measured by either isotope ratio mass spectrometry (IRMS, sample amount larger than 5 ml) or a cavity ring-down spectroscope (CRDS, sample amount less than 5 ml). The analytical precision of the IRMS is ±0.05‰ for $\delta^{18}O$ and ±0.7‰ for δD, and the CRDS provides a precision of ±0.1‰ for $\delta^{18}O$ and ±0.5‰ for δD. There were no

precipitation isotope measurements made during November 2009 and December 2010. Daily 2 m temperature was derived from an automatic weather station (AWS).

2.2.2. Surface Vapor Isotopes at Dome C and Kohnen Station

Casado et al. (2016) provided 23 days of hourly vapor isotope measurements at Concordia station between December 2014 and January 2015. Water vapor was pumped from 2 m above the surface for measurements. As regular calibration was not possible in the field and only a series of calibrations were conducted in the lab, measurement uncertainties are 1‰ for $\delta^{18}O$ and 6‰ for δD. Temperatures were measured near the spectrometers using HMP155 thermohygrometers at 2.58 m above the surface.

Ritter et al. (2016) measured vapor isotopes at Kohnen station for 35 days between December 2013 and January 2014. Kohnen station is located in Dronning Maud Land on the Antarctic Plateau (75°00′ S, 0°04′ E, 2892 m above sea level, Figure A1). Three inlets at heights of 0.2, 0.9, and 3 m were used to pump air alternatively every 11 min. Data from the top inlet are used here to estimate daily averages, which are set as missing values if there are less than 20 data points per day. After calibration, the measurement precision was estimated to be 0.9‰ for $\delta^{18}O$ and 3.0‰ for δD. Hourly 2 m temperature was available from an AWS.

2.2.3. Ocean Surface Vapor Isotopes

Kurita et al. (2016) measured water vapor isotopes along the Japanese Antarctic Research Expedition (JARE) cruise between Australia and Syowa station. The observations were extended from 2013 to 2020 for seven austral summers. Air samples were collected from 30 m above the sea surface. The analytical uncertainty was 0.28‰ for $\delta^{18}O$ and 2.5‰ for δD.

Thurnherr et al. (2020) observed water vapor isotopes from November 2016 to April 2017 during the Antarctic Circumnavigation Expedition (ACE). Isotope compositions of water vapor were measured at heights of 8 and 13.5 m, and the latter is used for analysis here.

Bonne et al. (2019) recorded water vapor isotopes for two years from Jun 2015 to Jul 2017 from the Arctic to the Southern Ocean on board the research vessel Polarstern. Air samples were extracted from 29 m above the sea surface. The measurement accuracy was estimated as 0.16‰ for $\delta^{18}O$ and 0.8‰ for δD.

From these three data sets, we calculate daily vapor isotopes for analysis. To evaluate the model performance, we exclude parts of the data sets to avoid the impacts of land and sea ice based on three criteria: (a) an observation must be located in an ocean grid cell of the ECHAM6-wiso model; (b) an observation must be located in a grid cell without sea ice, where sea ice values were derived from the ERA5 reanalysis (Hersbach et al., 2020); (c) an observation must be located between 20°S and 60°S. In total, we include 208 daily observations during extended austral summers from November to April, 78 of which are from Kurita et al. (2016), 62 from Thurnherr et al. (2020), and 68 from Bonne et al. (2019). The spatial distribution of the selected daily observations is shown in Figure A1.

2.3. Partial Correlation Analysis

Correlation analysis between two variables may produce misleading results if a third variable is related to both variables of interest. Therefore, a partial correlation analysis is used to quantify the degree of association between two variables, with the effect of a third variable removed. The partial correlation coefficients and associated p-values are calculated on the basis of the inverse covariance matrix (Kim, 2015). Partial correlation analysis qualitatively aligns with multiple linear regression; significant partial correlations correspond to non-zero coefficients in the regression results.

3. Results

3.1. Evaluation of Model Performance

First, we evaluate the performance of the ECHAM6-wiso model to identify any bias that could affect our subsequent findings. Here, we only show the results for δD and $d_{\ln}$, as those for $\delta^{18}O$ and d_{xs} share similar patterns.

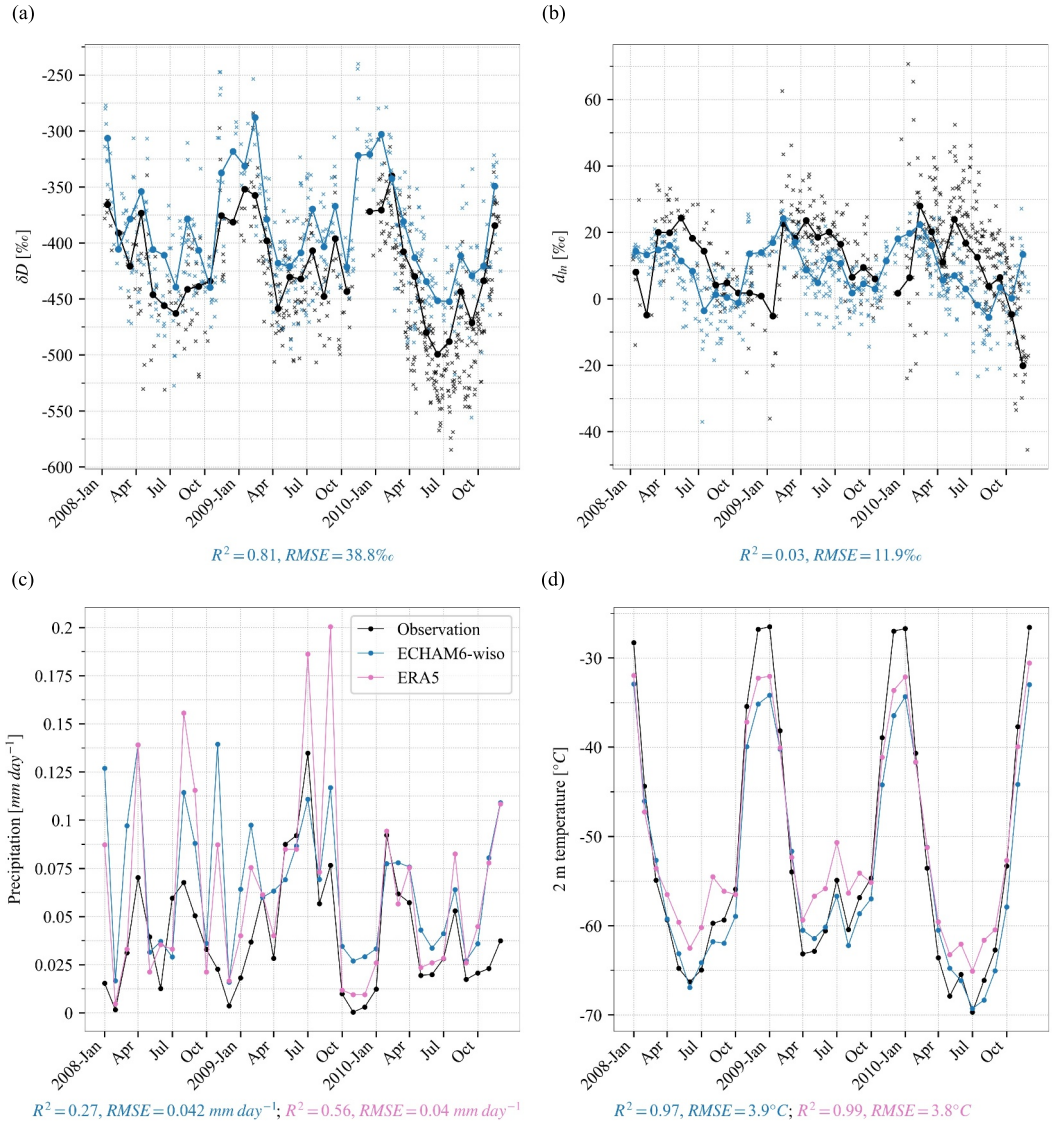

Figure 1. Monthly (a) δD in precipitation, (b) d_{ln} in precipitation, (c) precipitation, and (d) 2 m temperature at Dome C from Stenni et al. (2016), the ECHAM6-wiso *control* simulation, and the ERA5 reanalysis. (a) δD and (b) d_{ln} in daily precipitation (>0.02 mm day^{-1}) from Stenni et al. (2016) and ECHAM6-wiso are shown as crosses. R^2 values and RMSE between the monthly observations and the other two data sets are provided below each plot. As shown in panel (c), observations are in black, ECHAM6-wiso output in blue, and ERA5 is pink.

3.1.1. Observed Versus Simulated Precipitation Isotopes at Dome C

The annual cycle of observed monthly precipitation δD at Dome C is well captured by the *control* simulation, with a high R^2 value of 0.81 (Figure 1a). However, the *control* simulation exhibits consistent positive bias in monthly precipitation δD at Dome C (up to 69‰ in February 2009). The observed annual precipitation δD is overestimated by 43‰ (−371‰ vs. −414‰). These results are consistent with those of Ollivier et al. (2024, see their Fig. 6c) and 6Dreossi et al. (2023, see their Fig. 6), where they use an ERA5-nudged ECHAM6-wiso simulation at a horizontal resolution 0.9° × 0.9° from Cauquoin and Werner (2021) and daily precipitation isotope observations at Dome C from 2017 to 2021 and 2008–2017, respectively. The overestimation of precipitation δD at Dome C in the ECHAM6-wiso model resembles the overestimation of $\delta^{18}O$ in Antarctic precipitation, surface snow, and ice cores as reported by other GCM results (Cauquoin et al., 2019; Risi et al., 2010; Stenni et al., 2016).

The range of observed monthly precipitation d_{ln} at Dome C is reproduced by the *control* simulation, except the extremely low observed value in December 2010 (Figure 1b). The model-data differences range from −18‰ to 34‰, resulting in an RMSE of 11.9‰ (Figure 1b). The observed annual cycle in d_{ln} is poorly captured by the *control* simulation, indicated by a R^2 value of 0.03. The simulated seasonality appears to lead the observed one by a few months; the R^2 value increases to 0.67 for a 3-month lagged correlation. This may suggest an impact of continental recycling on the observed seasonal cycle, which is not captured by the ECHAM model. The potential causes of the model bias are investigated in the following.

Both the *control* simulation and the ERA5 reanalysis overestimate observed annual precipitation by ∼60% (23.2 and 24.3 vs. 14.5 mm year^{-1}, Figure 1c) at Dome C. This is consistent with the overestimation of Antarctic precipitation by almost all CMIP5 models compared to CloudSat observations, which may be linked to sea ice distribution (Palerme et al., 2017). The precipitation bias may be partly responsible for the precipitation isotope bias.

For surface temperatures, the *control* simulation shows a large cold bias in austral summer at Dome C (up to −9.5°C in December 2009, Figure 1d). As the annual mean surface temperature and δD of surface snow at sites in Antarctica are positively correlated (Masson-Delmotte et al., 2008), the negative temperature bias cannot explain the positive bias in precipitation δD.

3.1.2. Observed Versus Simulated Surface Vapor Isotopes at Dome C and Kohnen Station

The *control* simulation overestimates observed δD of daily surface vapor at both Dome C and Kohnen station (Figures 2a and 2b). The positive bias in the vapor δD may be related to the positive bias in precipitation δD (Figure 1a), as a considerable fraction of the precipitation at Dome C is formed from the surface vapor as hoar frost (Stenni et al., 2016). Since Casado et al. (2016) find a significant positive correlation between daily vapor δD and 3 m temperature at Dome C, the positive bias in vapor δD is not attributable to the negative temperature bias (Figures 2g and 2h). Some of the bias in vapor δD may be related to the bias in specific humidity (Figures 2e and 2f), as potential model bias in moisture sources, mixing, and transport can affect both specific humidity and vapor δD.

The observed d_{ln} of daily surface vapor at both Dome C and Kohnen station is considerably underestimated in the *control* simulation (Figures 2c and 2d). The variability of daily observed d_{ln} at Dome C is also underestimated by the *control* simulation (14.2‰ vs. 3.7‰ for 1σ). These model-data discrepancies in vapor isotopes cannot be resolved by adjusting parameters related to kinetic fractionation (Figure A2). Modifying the parameters induces parallel shifts in the simulated δD and d_{ln}, which partly reduces the RMSE for d_{ln} but has limited impacts on δD.

3.1.3. Observed Versus Simulated Ocean Surface Vapor Isotopes

Similar model-data discrepancies for surface vapor at Dome C and Kohnen Station are reported for Greenland surface vapor $\delta^{18}O$ and d_{xs} and were previously attributed to a model bias in marine boundary layer vapor isotopes (Steen-Larsen et al., 2017). To investigate this aspect in our simulation, we evaluate the performance of the ECHAM6-wiso model in simulating the daily ocean surface vapor isotopes reported in the Antarctic realm by Kurita et al. (2016), Thurnherr et al. (2020) and Bonne et al. (2019, Section 2.2.3), where most of the Antarctic precipitation originates from Gao et al. (2024). We find a good model-data agreement for daily ocean surface vapor and its isotope compositions with respect to R^2 values and RMSE (Figure 3). Therefore, the model bias in precipitation and vapor isotopes at Dome C cannot be explained by bias in ocean surface vapor. This implies that the bias in modeled precipitation deuterium excess at Dome C may result from moisture transport, mixing, precipitation formation in clouds, and the influence of moisture evaporative sources.

3.2. Moisture Source Controls on Deuterium Excess

The previous section shows that it is challenging for isotope-enabled GCMs to accurately simulate all aspects of Antarctic precipitation isotope ratios, particularly deuterium excess (Cauquoin et al., 2019; Risi et al., 2010; Stenni et al., 2016). Although the *control* simulation shows a large negative bias compared to the 28-day observations of surface vapor d_{ln} at Dome C, the amplitude and variability of the observed monthly precipitation d_{ln} over 3 years are largely captured by the *control* simulation with a three-month lead time. The model performs well in simulating ocean surface vapor isotopes over the evaporative source regions for Antarctic precipitation. This

Figure 2. Summer daily (a, b) δD in surface vapor, (c, d) $d_{\ln}$ in surface vapor, (e, f) specific humidity, and (g, h) 2 m temperature at (a, c, e, g) Dome C from Casado et al. (2016) and (b, d, f, h) Kohnen station from Ritter et al. (2016), as well as from the ECHAM6-wiso *control* simulation and the ERA5 reanalysis. As shown in panel (e) observations are in black, ECHAM6-wiso output in blue, and ERA5 is pink.

gives us confidence in the modeled relationships between moisture source properties and vapor $d_{\ln}$. We now use the moisture source information from newly developed water tracing diagnostics by Gao et al. (2024) in the ECHAM6-wiso model to further explore climate controls on deuterium excess.

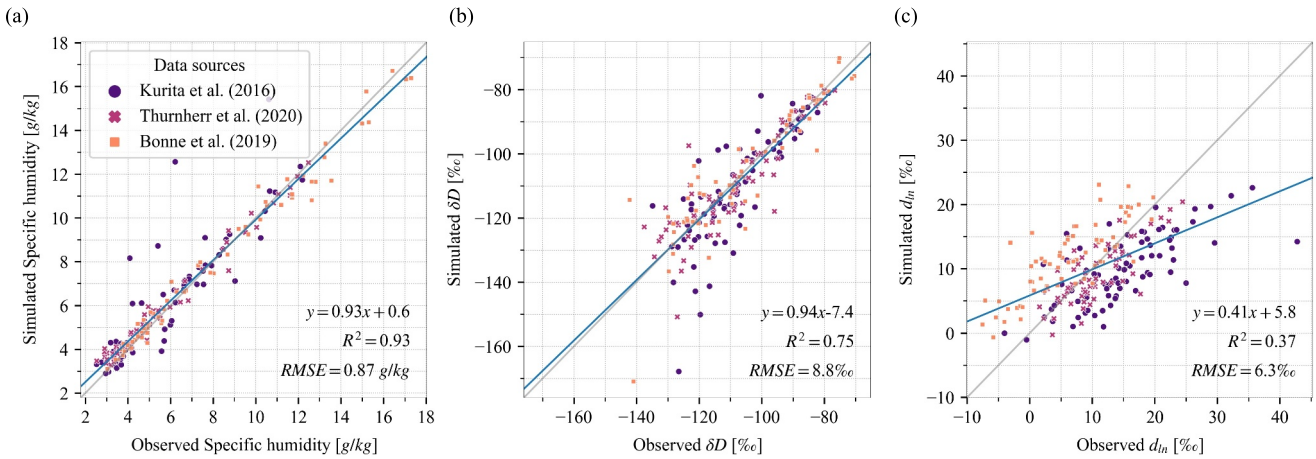

Figure 3. Summer daily (a) specific humidity, (b) δD in surface vapor, and (c) $d_{\ln}$ in surface vapor over the ocean from November 2013 to March 2020 in the ECHAM6-wiso *control* simulation and the three data sets (Bonne et al., 2019; Kurita et al., 2016; Thurnherr et al., 2020). Locations of the observations are shown in Figure A1.

3.2.1. Source SST Versus Other Source Properties of Dome C Precipitation

Given the debate surrounding controls on deuterium excess (Pfahl & Sodemann, 2014), we use modeling results from the ECHAM6-wiso model to evaluate those controls. Correlation analysis indicates significant correlations between $d_{\ln}$ and the moisture source properties of precipitation at Dome C in the *control* simulation (Table 2). The low R^2 values at the daily timescale result from days with very low precipitation amount: if we exclude days with less than 0.02 mm precipitation, the R^2 value between $d_{\ln}$ and source SST increases to 0.59 on the daily timescale. Removing monthly climatology values from monthly data (i.e., monthly anomalies) reveals the impacts of the annual cycle, which are limited for source SST.

However, the relationships shown in Table 2 may be confounded by the effect of a third variable (Section 2.3). In fact, partial correlation analysis reveals that it is source SST rather than other source properties that has a causal relationship with $d_{\ln}$ of precipitation at Dome C in the *control* simulation (Table 3). While controlling (i.e., removing the effect of) the source SST, partial correlations between $d_{\ln}$ and other source properties of precipitation at Dome C are negligible at all timescales. In contrast, while controlling other source properties, there are significant partial correlations between $d_{\ln}$ and source SST on every timescale. These findings also apply to d_{xs} and the whole continent (not shown).

3.2.2. Source SST Versus RHsst of Ocean Surface Vapor

The weak correlation between source RHsst and deuterium excess is in contradiction to the results of Pfahl and Sodemann (2014). Since the isotope compositions of ocean surface evaporation fluxes are parameterized after Craig and Gordon (1965) in the ECHAM6-wiso model (Hoffmann et al., 1998), deuterium excess in the evaporation fluxes is controlled by both SST and RHsst (Merlivat & Jouzel, 1979). As RHsst is related to SST, a partial correlation analysis is conducted to explore their impacts on $d_{\ln}$ for both Antarctic precipitation and ocean surface vapor from where most of Antarctic precipitation originates (Figure 4). Although $d_{\ln}$ in annual ocean surface vapor is strongly negatively correlated with source RHsst while controlling source SST (Figure 4a), the strong correlation vanishes for Antarctic precipitation (Figure 4b) along poleward moisture transport (Figure A3a). In contrast, positive partial correlations between $d_{\ln}$ and source SST while controlling source RHsst persist from ocean surface vapor to Antarctic precipitation (Figures 4c, 4d, and Figure A3b). These findings remain valid for daily to seasonal timescales (not shown).

The negative partial correlations between $d_{\ln}$ and source SST while controlling source RHsst over parts of the Southern Ocean are contrary to the expected positive correlation in surface evaporation fluxes (Figure 4c). The negative partial correlations become more evident on the daily timescale (Figure 5).

Table 2
Correlations Between $d_{\ln}$ and Source Properties of Precipitation at Dome C in the ECHAM6-Wiso control Simulation

Correlation (R^2)		Annual	Monthly	Monthly anomalies	Daily
$d_{\ln}$	Source SST	0.79	0.83	0.61	0.28
	Source rh2m	0.27	0.05	0.49	0.07
	Source vel10	0.5	0.64	0.16	0.18
	Source RHsst	0.01	0.11	0.21	0.02

Note. Correlation values with a p-value > 0.01 are indicated in gray.

Table 3
Partial Correlations Between d_{ln} and Source Properties While Controlling Another Source Property of Precipitation at Dome C in the ECHAM6-Wiso control Simulation

Partial correlation (R^2)		Controlling	Annual	Monthly	Monthly anomalies	Daily
d_{ln}	Source rh2m	Source SST	0.02	0.02	0.07	0
	Source vel10		0.01	0.04	0.01	0
	Source RHsst		0	0.03	0.04	0.01
	Source SST	Source rh2m	0.72	0.83	0.28	0.23
		Source vel10	0.58	0.56	0.54	0.13
		Source RHsst	0.79	0.82	0.53	0.28

Note. Correlation values with a p-value > 0.01 are indicated in gray.

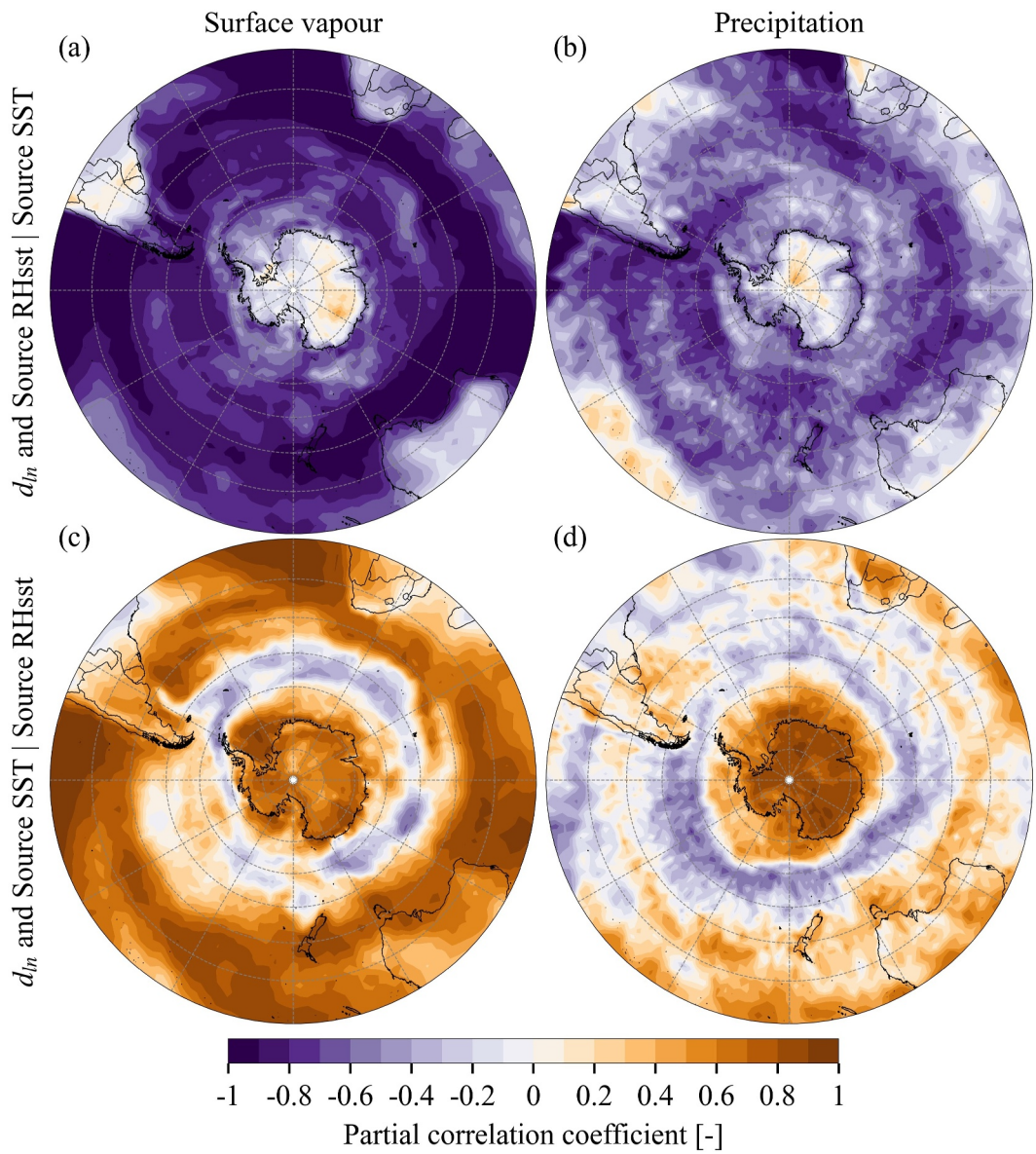

Figure 4. Partial correlations between annual d_{ln} and (a–b) source RHsst while controlling source SST and (c–d) source SST while controlling source RHsst. Results in (a, c) show correlations in surface vapor and (b, d) show correlations in precipitation in the ECHAM6-wiso *control* simulation.

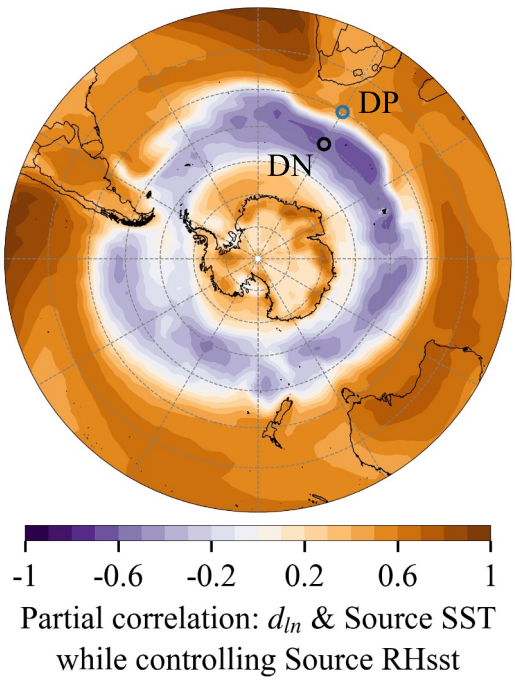

Figure 5. Partial correlations between daily $d_{\ln}$ and source SST while controlling source RHsst of surface vapor in the ECHAM6-wiso *control* simulation. The blue and black circles indicate two nearby sites used for further analysis, that is, DP and DN with positive and negative partial correlations, respectively.

This finding is in contrast to the observational study of Bonne et al. (2019), which find a positive partial correlation between d_{xs} of ocean surface vapor and local SST while controlling local RHsst. Their finding is confirmed using data from Kurita et al. (2016, Fig. A4a), indicated by a positive coefficient before SST in the regression equation (multiple linear regression using d_{xs} gives similar results: $d_{xs} = -0.27RHsst + 0.39SST + 25.3$). Using corresponding daily data from the *control* simulation, we obtain qualitatively consistent results for both local and source RHsst and SST (Figures A4b and A4c). Although the data in Figure A4 have a broad spatial coverage, the analysis in Figure 5 is performed at each grid cell. Thus, our results indicate a difference between spatial and temporal deuterium excess and SST relationships. Similar reversed relationships between deuterium excess and SST were found in Aemisegger and Sjolte (2018, see their Fig. 7c). They attributed the pattern to cold air outbreaks and strong large-scale ocean evaporation events, as strong evaporation into the cold air results in high deuterium excess and evaporative cooling of the ocean surface. Although their study does not check the partial correlation while controlling the effect of RHsst, the feedback between evaporation and SST is certainly an interesting question to investigate in future studies.

The negative partial correlations between $d_{\ln}$ and source SST while controlling source RHsst are further investigated by analyzing two nearby sites, DP and DN (Figure 5), which exhibit positive and negative partial correlations, respectively. To explore physical controls on ocean surface vapor $d_{\ln}$ in addition to RHsst, we look at the residuals in the regression $d_{\ln} = f(RHsst)$. In DP, the residuals in the regression $d_{\ln} = f(RHsst)$ decrease with increasing source SST (Figure 6a). This is expected as SST exerts a positive control on $d_{\ln}$ in evaporative fluxes; therefore, the regression using only source RHsst would underestimate $d_{\ln}$ at relatively high source SST. It also applies to DN when source SST is less than ~7°C, but breaks down when source SST is larger than ~10°C (Figure 6b). In fact, although excluding daily data that exceed an upper threshold of source SST, the partial correlation at DN increases from negative to positive with lower upper thresholds (Figure A5). This suggests that the negative partial correlation at DN results from relatively high source SST days. As days with high source SST values at DN are almost always associated with precipitation (Figure A6), the impact of precipitation processes on the relationship between deuterium excess and SST should be investigated in future studies. For instance, water tracers designated for condensation properties during cloud formation as used in Dütsch et al. (2019, see their Sec. 2.3) can be used to separate effects of physical processes before and after condensation processes.

3.2.3. Logarithmic Versus Linear Definitions of Deuterium Excess

A key research question remains: which definition of deuterium excess should be used for the reconstruction of moisture source conditions from Antarctic ice cores? The results here show that $d_{\ln}$ is a better proxy than d_{xs} for source SST of Antarctic precipitation. $d_{\ln}$ shows stronger correlations with source SST than d_{xs} for precipitation at Dome C in the *control* simulation from daily to annual timescales (Table 4). These findings at Dome C are valid across Antarctica. For example, for annual precipitation over Antarctic regions above 2,250 m elevation, source SST is always more strongly correlated with $d_{\ln}$ (R^2 values range from 0.58 to 0.93, Figure 8a) than d_{xs} (R^2 values range from 0.3 to 0.91).

3.2.4. Regression Between Source SST and $d_{\ln}$

The modeled relationships between $d_{\ln}$ and source SST may be useful for interpreting Antarctic ice cores. Previous studies have combined $d_{\ln}$ and d_{xs} with δD for the reconstruction of source SST (Landais et al., 2021), which is evaluated here. Although controlling d_{xs} of Dome C precipitation in the *control* simulation, partial correlations between δD and source SST are even stronger than the corresponding correlations at every timescale (Table 5). In contrast, although controlling $d_{\ln}$, partial correlations between δD and source SST are close to 0 on every timescale. Consequently, the strong predictive performance for source SST using $d_{\ln}$ cannot be further improved

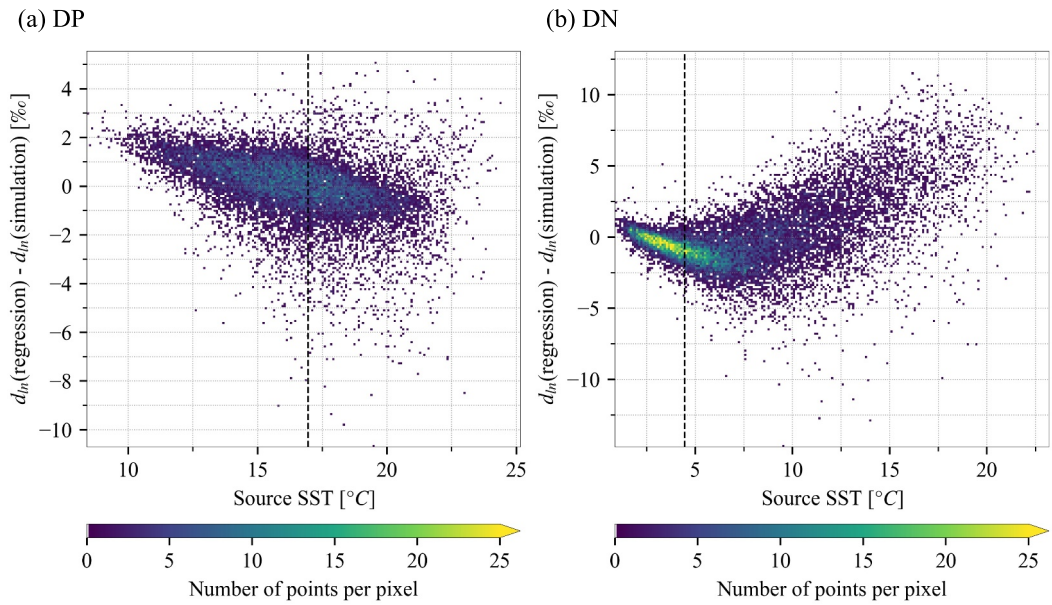

Figure 6. Density plots between residuals in the regression daily $d_{\ln} = f(RHsst)$ and source SST at (a) DP and (b) DN in the ECHAM6-wiso *control* simulation. The vertical black dashed lines represent the annual mean site SST. The residual is defined as the difference between estimated $d_{\ln}$ based on the linear regression and the simulated $d_{\ln}$.

by δD (Figure 7a), but the prediction based on d_{xs} can be improved by δD (Figures 7b and 7c). These findings also apply to daily to seasonal timescales (not shown). As multiple linear regression increases the risk of overfitting, that is, the model fits not only the underlying relationship but also the noise (Lever et al., 2016), we suggest using $d_{\ln}$ instead of the combination of d_{xs} and δD for the reconstruction of source SST.

To check the consistency of the modeled relationship between $d_{\ln}$ and source SST at Dome C, we investigate its spatial variations throughout Antarctica (Figure 8). In most of inland Antarctica, the R^2 values between the simulated and estimated source SST using $d_{\ln}$ of annual precipitation are greater than 0.5 in the *control* simulation, and the corresponding RMSE are less than 0.5°C (Figures 8a and 8b). In Antarctic regions above 2,250 m elevations, the slope in the linear equation $source\ SST = f(d_{\ln})$ decreases from 0.80 to 0.23°C/‰ towards the interior (Figure 8c). It suggests that simulated $d_{\ln}$ of annual precipitation is more sensitive to source SST in more inland regions (as a unit change in moisture source SST would induce a larger change in $d_{\ln}$ of annual precipitation in inland than coastal regions). This finding is qualitatively consistent with the results of Vimeux et al. (2001). It may result from the different moisture transport pathways, which should be investigated in future studies.

To assess the sensitivity of the modeled relationships between $d_{\ln}$ and source SST for various parameters in the ECHAM6-wiso model related to kinetic fractionation, we repeat the linear regression analysis using the results of the model sensitivity experiments (Table 1). From this analysis (Table 6), we find the following: (a) Linear regression parameters in $source\ SST = f(d_{\ln})$ are insensitive to the kinetic fractionation coefficient k (*k52* and *k43*). (b) R^2 values and RMSE between the simulated and estimated source SST are insensitive to the intercept of the supersaturation function defined in ECHAM6-wiso; however, the slope in $source\ SST = f(d_{\ln})$ increases with a reduction in the intercept of the supersaturation function, and vice versa (*I01* and *I03*). This implies that a reduction in absolute supersaturation values leads to a decreased sensitivity of $d_{\ln}$ to source SST. (c) Decreasing the slope of the supersaturation function in *S3* leads to a lower R^2 value, a higher RMSE, and a larger slope with a wider 95% confidence interval compared to the *control* simulation. Increasing the slope of the supersaturation function in *S6* does not change R^2 values or RMSE notably, but results in a reduced slope compared to the *control* simulation. This suggests that when the supersaturation function has a reduced sensitivity to the condensation temperature, $d_{\ln}$ becomes less sensitive to source SST. It clearly indicates that the correlation between $d_{\ln}$ and

Table 4
Correlation Between Deuterium Excess and Source SST of Precipitation at Dome C in the ECHAM6-Wiso control Simulation

Correlation (R^2)		Annual	Monthly	Monthly anomalies	Daily
$d_{\ln}$	Source SST	0.79	0.83	0.61	0.28
d_{xs}	Source SST	0.48	0.44	0.26	0.15

Note. All correlation values are associated with a p-value < =0.01.

Table 5
Partial Correlations Between Source SST and Isotope Parameters While Controlling Another Isotope Parameter of Precipitation at Dome C in the ECHAM6-Wiso control Simulation

Partial correlation (R^2)		Controlling	Annual	Monthly	Monthly anomalies	Daily
Source SST	d_{ln}	δD	0.66	0.72	0.52	0.18
	d_{xs}		0.7	0.74	0.55	0.35
	δD	d_{ln}	0	0.01	0	0
		d_{xs}	0.65	0.72	0.51	0.34
Correlation (R^2):	δD	Source SST	0.38	0.41	0.19	0.14

Note. Correlations between δD and source SST are also provided. Correlation values with a p-value > 0.01 are indicated in gray.

source SST is strongly modulated during transport. Overall, we conclude that the predefined supersaturation function in mixed phase and ice clouds in ECHAM6-wiso is the main control on the sensitivity of the modeled relationship between d_{ln} and source SST.

4. Conclusions

In Antarctic ice cores, deuterium excess has been shown to reflect source SST and RHsst during evaporation (Landais et al., 2021). However, d_{xs} and d_{ln} may be modified by additional processes, such as condensation, rain reevaporation, or vapor mixing. To better understand evaporative source properties, this study therefore examines the problem using moisture source information from newly developed water tracers in the ECHAM6-wiso model (Gao et al., 2024).

Water isotopes in Antarctic precipitation and surface vapor from central Antarctic stations are used to evaluate the performance of the ECHAM6-wiso model. Compared to observations, this analysis shows that the ERA5-nudged ECHAM6-wiso simulations exhibit a positive bias in precipitation and vapor δD and a negative bias in vapor d_{ln} at Dome C. This bias does not appear to stem from temperature or ocean surface vapor isotope biases, nor can it be mitigated by adjusting kinetic-fractionation parameters or increasing the spatial resolution of the model (Cauquoin & Werner, 2021). We hypothesize that this bias may result from deficiencies in other aspects of the ECHAM6 model's hydrological cycle, such as cloud formation under supersaturated conditions, or the lack of some isotopic processes, such as fractionation during surface sublimation of water isotopes over Antarctica (Dietrich et al., 2023; Ollivier et al., 2024; Pang et al., 2019; Wahl et al., 2021). Despite these biases and some noise, the ECHAM6-wiso model does capture the variations of monthly precipitation δD and the amplitude of monthly precipitation d_{ln} with 3 months lag time at Dome C. Over the ocean surrounding Antarctica, there is a good model-data agreement for daily ocean surface vapor and its isotope compositions, compared to the data sets

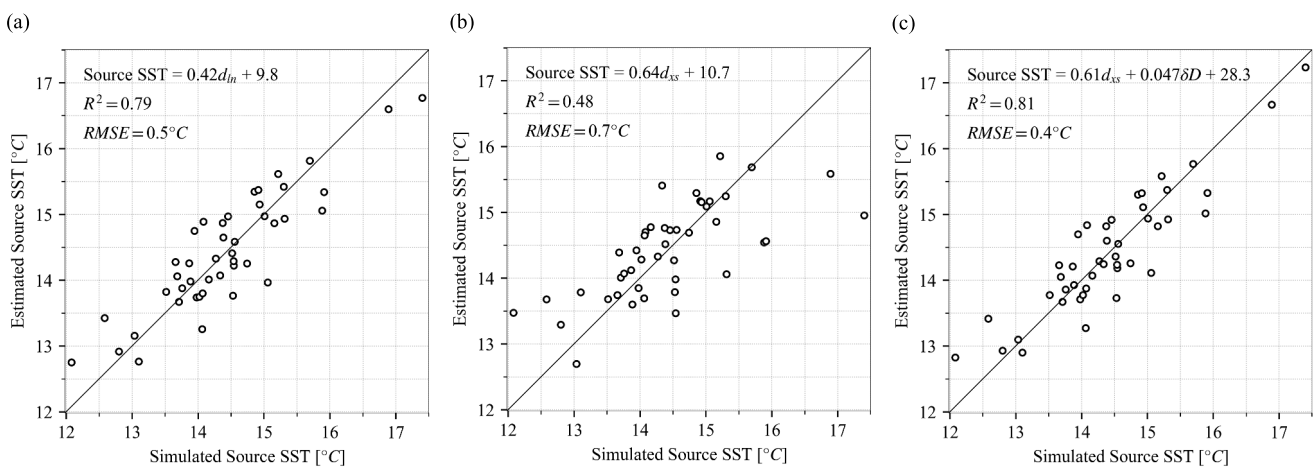

Figure 7. Regression of annual source SST with (a) d_{ln}, (b) d_{xs}, and (c) d_{xs} and δD of precipitation at Dome C in the ECHAM6-wiso *control* simulation. The estimated source SST is calculated based on the regression. R^2 values and RMSE between simulated and estimated source SST are given.

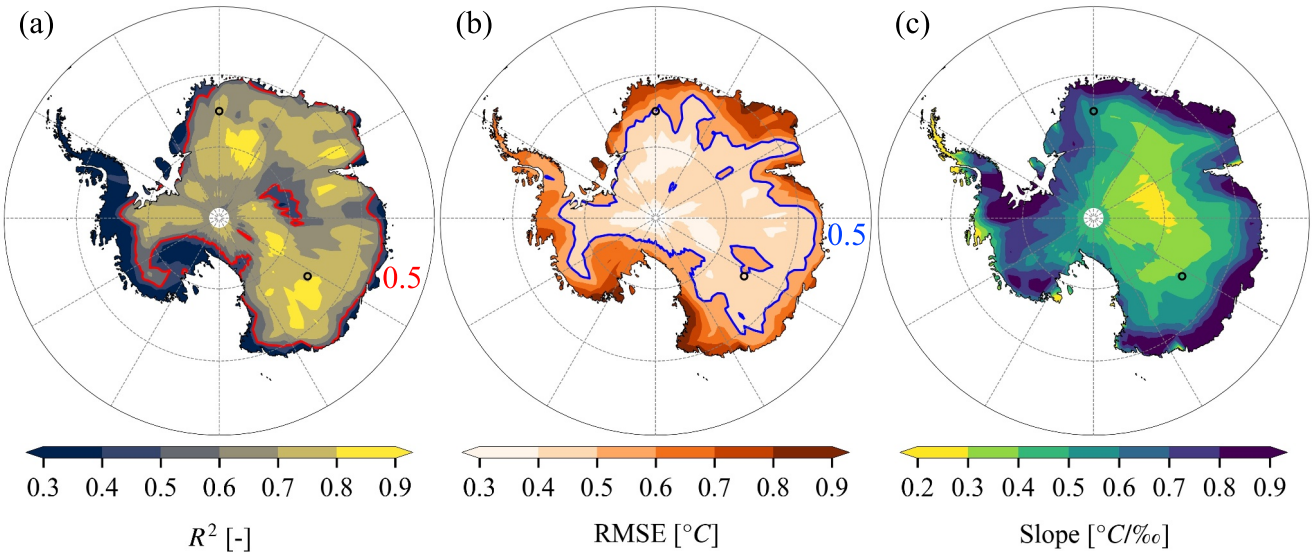

Figure 8. Linear regression parameters between source SST and d_{ln} of annual precipitation at each grid cell over Antarctica in the 44-year ECHAM6-wiso *control* simulation. (a) R^2 values and (b) RMSE between simulated and estimated source SST. (c) The slope in the linear equation *source SST* $= f(d_{ln})$. Red contours in panel (a) and blue contours in panel (b) represent $R^2 = 0.5$ and $RMSE = 0.5$°C, respectively.

of Kurita et al. (2016), Thurnherr et al. (2020), and Bonne et al. (2019). These provide some confidence in the simulated relationships between d_{xs} and d_{ln} and evaporative source properties.

Overall, the modeling results support previous studies that showed it is possible to reliably recover information on evaporative source properties, particularly SST changes, from d_{ln} in Antarctic precipitation (Landais et al., 2021; Vimeux et al., 2001). The results show that d_{ln} is a more reliable indicator of moisture source properties than d_{xs}, with source SST being the primary control of d_{ln} in Antarctic precipitation. Although RHsst influences d_{ln} in ocean surface evaporation fluxes, this influence diminishes quickly above the ocean. In contrast, positive partial correlations between d_{ln} and source SST, controlling for source RHsst, persist from the ocean surface to Antarctic precipitation, demonstrating that d_{ln} is primarily controlled by source SST.

About 80% of the variability in d_{ln} of annual precipitation at Dome C in the *control* simulation is associated with evaporative source changes in SST. This leads to a strong predictive performance for source SST using d_{ln}, with a RMSE of 0.5°C. The explained variance of d_{ln} by source SST for precipitation at Dome C is also notable on daily (28% using all days or 59% while excluding low precipitation days) to monthly scales (61 or 83%, depending on whether monthly climatology is removed), suggesting the potential to recover moisture source information from observed precipitation isotopes at different timescales, particularly for extreme precipitation events. Although the R^2 values between source SST and d_{ln} are larger on monthly than annual scales for Dome C precipitation (Table 2), the RMSE from the linear regression results are the smallest on the annual scale. Consistent with

Table 6
Sensitivity of Linear Regression Parameters Between Source SST and d_{ln} of Annual Precipitation at Dome C to Kinetic-Fractionation-Related Parameters in the Seven ECHAM6-Wiso Simulations Described in Table 1

Experiments	R^2	RMSE [°C]	Slope [°C/‰]	95% confidence interval of the slope [°C/‰]
control	0.79	0.5	0.42	[0.35, 0.48]
k52	0.79	0.5	0.41	[0.35, 0.48]
k43	0.79	0.5	0.42	[0.35, 0.48]
I01	0.76	0.5	0.47	[0.39, 0.55]
I03	0.79	0.5	0.37	[0.31, 0.43]
S3	0.46	0.7	0.48	[0.32, 0.64]
S6	0.77	0.5	0.28	[0.23, 0.33]

Vimeux et al. (2001), results shown here indicate that d_{ln} in annual precipitation is more sensitive to source SST in inland regions compared to coastal regions. Given the risk of overfitting with multiple linear regression, we recommend recovering past evaporative source SST information from d_{ln} alone, rather than combining d_{xs} and δD. Given the challenges in accurately modeling deuterium excess, there are clearly uncertainties in the model's derived statistics between deuterium excess and source properties of Antarctic precipitation. However, some confidence in our general key conclusions can be provided given that there is some model-observation agreement for deuterium excess (especially at the precipitation source) and that the source location of Antarctic precipitation in the model agrees with other studies (Gao et al., 2024). In the future, it would clearly be beneficial to compare these ECHAM6-wiso findings with similar studies using other models (e.g., comparable diagnostics are being developed in the Met Office Unified Model) and higher model resolution.

In future, if these insights are applied to precipitation derived from ice cores, it is important to consider that precipitation isotope signals can be altered by post-deposition processes (Casado et al., 2018; Steen-Larsen et al., 2014). Therefore, further examination of post-depositional processes and their effect on d_{ln} would be valuable. We also observe higher partial correlations between source SST and d_{ln} while controlling source RHsst for Antarctic precipitation than Antarctic surface vapor (Figure 4d vs. Figure 4c), which may be more affected by surface isotope fluxes. Additionally, as the relationship between d_{ln} and source SST may vary under different climate conditions, further paleoclimate modeling is needed, ideally along with additional investigation into the model-observation discrepancies identified in our present-day simulations.

Finally, we uncover an important control on d_{ln} in vapor above the Southern Ocean, which may be driven by cold air outbreaks or precipitation processes. This is visible in the region of unexpected negative partial correlation between daily d_{ln} in vapor and source SST while controlling source RHsst over the Southern Ocean (Figure 5, blue band). This suggests that d_{ln} in vapor may contain useful information on synoptic weather regimes or precipitation processes in this region. Future investigations could provide insights into hydrological processes in this understudied region.

Appendix A: Additional Figures and Tables

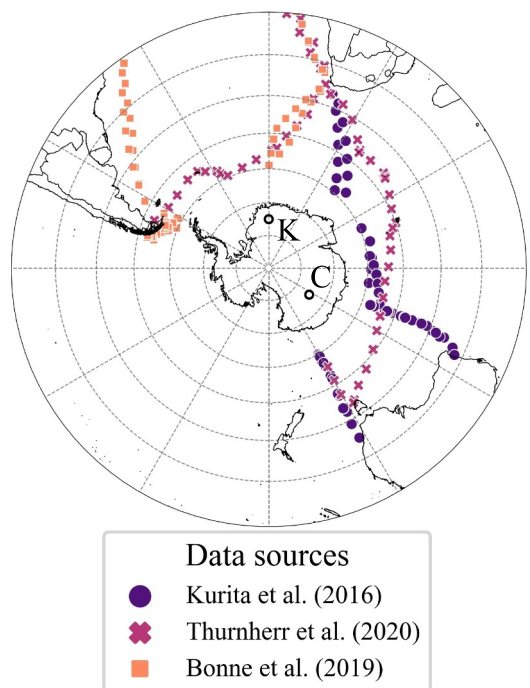

Figure A1. Spatial distribution of the 208 daily ocean surface vapor isotope observations from the three data sets (Bonne et al., 2019; Kurita et al., 2016; Thurnherr et al., 2020). Locations of Dome C and Kohnen station are marked by black circles and labeled as C and K, respectively.

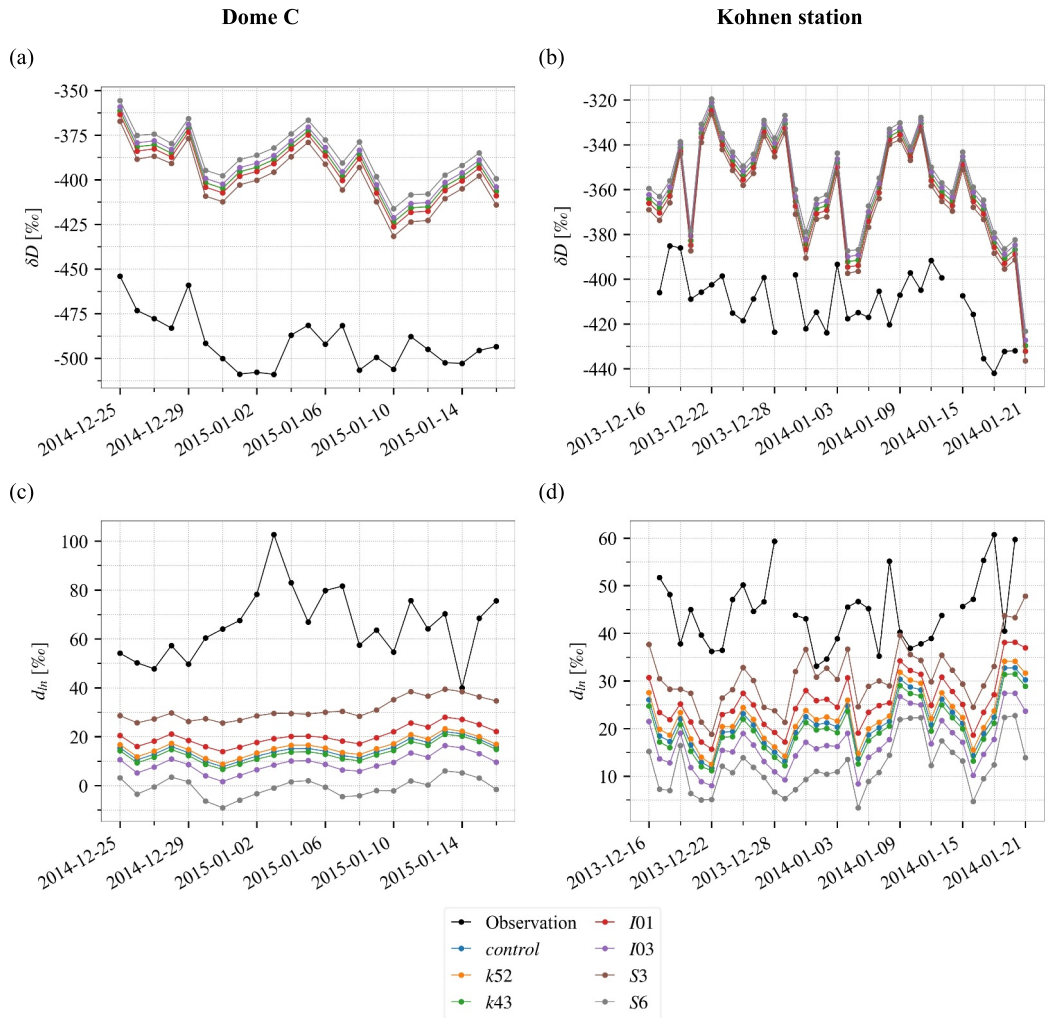

Figure A2. Summer daily (a, b) δD and (c, d) $d_{\ln}$ in surface vapor at (a, c) Dome C from Casado et al. (2016) and (b, d) Kohnen station from Ritter et al. (2016), as well as from the seven ECHAM6-wiso simulations described in Table 1.

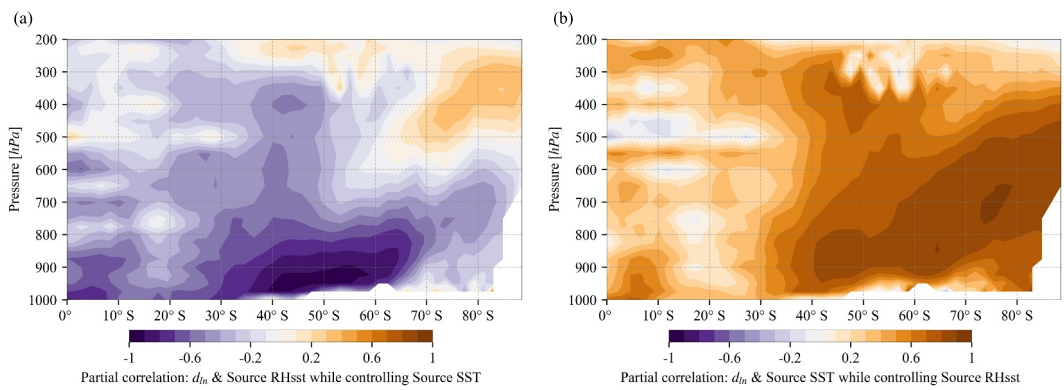

Figure A3. Partial correlations between annual $d_{\ln}$ and (a) source RHsst while controlling source SST and (b) source SST while controlling source RHsst in zonal mean vapor in the ECHAM6-wiso *control* simulation. The analysis on a meridional cross-section across Dome C shows similar patterns.

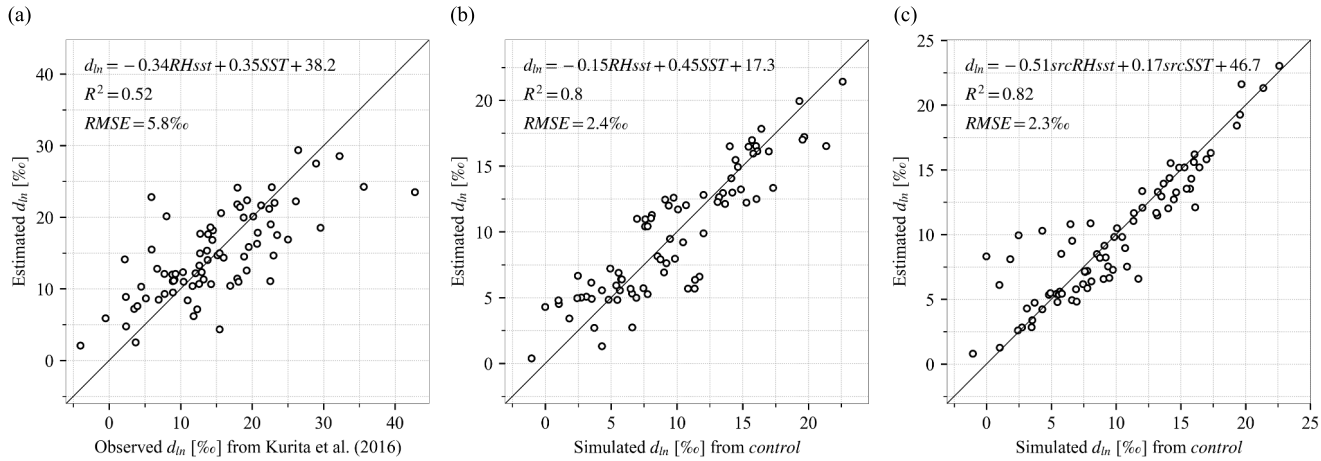

Figure A4. Multiple linear regression of daily d_{ln} with local or source RHsst and SST of ocean surface vapor. Daily data are from (a) Kurita et al. (2016) and (b–c) the ECHAM6-wiso *control* simulation at the same dates and sites as in panel (a). We use local RHsst and SST in panel (b) and source RHsst and SST in panel (c). Estimated d_{ln} is calculated based on the multiple linear regression.

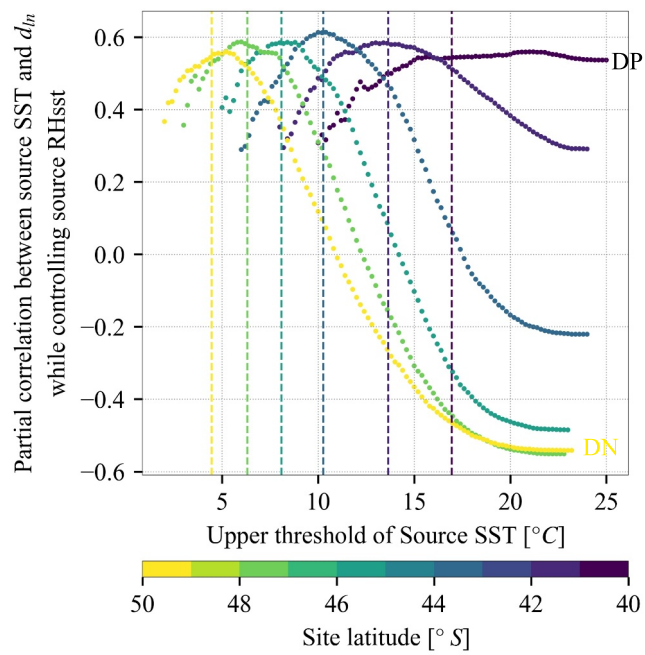

Figure A5. Variations of partial correlations between daily d_{ln} and source SST while controlling source RHsst of surface vapor with upper threshold of source SST in six grid cells from DP to DN in the ECHAM6-wiso *control* simulation. The vertical-colored dashed lines represent the annual mean site SST.

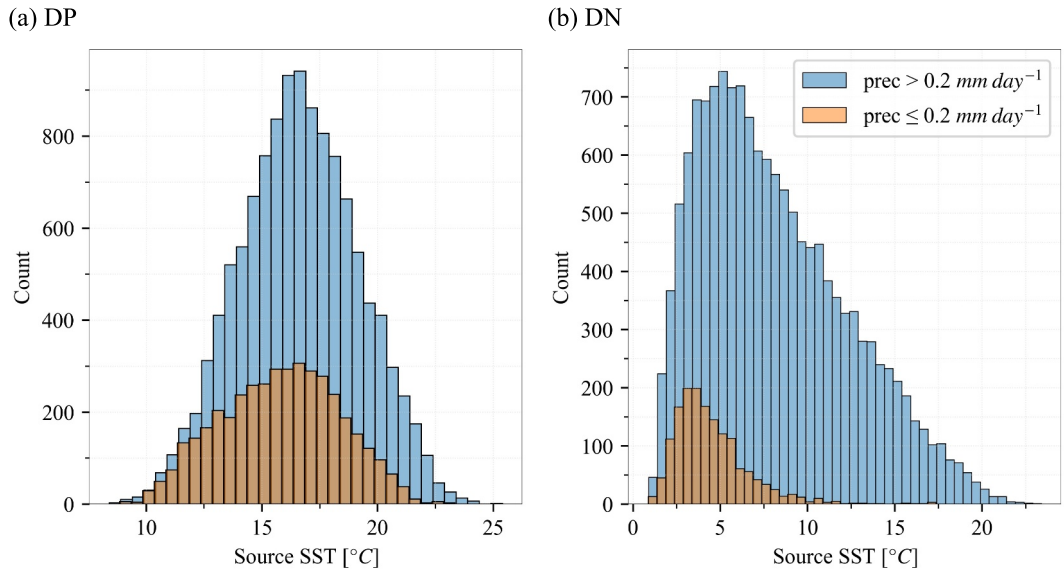

Figure A6. Histogram of source SST of daily surface vapor at (a) DP and (b) DN during precipitation and non-precipitation days in the ECHAM6-wiso *control* simulation.

Data Availability Statement

The ECHAM6-wiso model output and the code used for analysis can be found at Gao et al. (2025).

Acknowledgments
This publication was generated in the frame of the DEEPICE project. The project has received funding from the European Union's Horizon 2020 Research and Innovation Program under the Marie Sklodowska-Curie Grant Agreement No 955750. QG and MW acknowledge the technical support and computing resources provided by the AWI Computer and Data Center in setting up and running the ECHAM6-wiso simulations. QG acknowledges Alexandre Cauquoin in providing the spin-up simulation of ECHAM6-wiso. QG acknowledges the DEEPICE community in all useful discussions. Louise C. Sime was supported by the NERC National Capability International Research Program Surface Fluxes In Antarctica (SURFEIT): Grant Nos. NE/X009319/1, NE/X009386/1, and NE/P009271/1.

References

Aemisegger, F. (2018). On the link between the North Atlantic storm track and precipitation deuterium excess in Reykjavik. *Atmospheric Science Letters*, *19*(12), e865. https://doi.org/10.1002/ASL.865

Aemisegger, F., & Sjolte, J. (2018). A climatology of strong large-scale ocean evaporation events. Part II: Relevance for the deuterium excess signature of the evaporation flux. *Journal of Climate*, *31*(18), 7313–7336. https://doi.org/10.1175/JCLI-D-17-0592.1

Benetti, M., Reverdin, G., Pierre, C., Merlivat, L., Risi, C., Steen-Larsen, H. C., & Vimeux, F. (2014). Deuterium excess in marine water vapor: Dependency on relative humidity and surface wind speed during evaporation. *Journal of Geophysical Research: Atmospheres*, *119*(2), 584–593. https://doi.org/10.1002/2013JD020535

Bonne, J. L., Behrens, M., Meyer, H., Kipfstuhl, S., Rabe, B., Schönicke, L., et al. (2019). Resolving the controls of water vapour isotopes in the Atlantic sector. *Nature Communications*, *10*(1), 1–10. https://doi.org/10.1038/s41467-019-09242-6

Casado, M., Hébert, R., Faranda, D., & Landais, A. (2023). The quandary of detecting the signature of climate change in Antarctica. *Nature Climate Change*, *13*(10), 1082–1088. https://doi.org/10.1038/s41558-023-01791-5

Casado, M., Landais, A., Masson-Delmotte, V., Genthon, C., Kerstel, E., Kassi, S., et al. (2016). Continuous measurements of isotopic composition of water vapour on the East Antarctic Plateau. *Atmospheric Chemistry and Physics*, *16*(13), 8521–8538. https://doi.org/10.5194/ACP-16-8521-2016

Casado, M., Landais, A., Picard, G., Münch, T., Laepple, T., Stenni, B., et al. (2018). Archival processes of the water stable isotope signal in East Antarctic ice cores. *The Cryosphere*, *12*(5), 1745–1766. https://doi.org/10.5194/TC-12-1745-2018

Cauquoin, A., & Werner, M. (2021). High-resolution nudged isotope modeling with ECHAM6-Wiso: Impacts of updated model physics and ERA5 reanalysis data. *Journal of Advances in Modeling Earth Systems*, *13*(11), e2021MS002532. https://doi.org/10.1029/2021MS002532

Cauquoin, A., Werner, M., & Lohmann, G. (2019). Water isotopes - Climate relationships for the mid-Holocene and preindustrial period simulated with an isotope-enabled version of MPI-ESM. *Climate of the Past*, *15*(6), 1913–1937. https://doi.org/10.5194/cp-15-1913-2019

Chung, A., Parrenin, F., Steinhage, D., Mulvaney, R., Martiń, C., Cavitte, M. G., et al. (2023). Stagnant ice and age modelling in the Dome C region, Antarctica. *The Cryosphere*, *17*(8), 3461–3483. https://doi.org/10.5194/TC-17-3461-2023

Ciais, P., & Jouzel, J. (1994). Deuterium and oxygen 18 in precipitation: Isotopic model, including mixed cloud processes. *Journal of Geophysical Research*, *99*(D8), 16793–16803. https://doi.org/10.1029/94JD00412

Craig, H. (1961). Isotopic variations in meteoric waters. *Science*, *133*(3465), 1702–1703. https://doi.org/10.1126/SCIENCE.133.3465.1702

Craig, H., & Gordon, L. I. (1965). Deuterium and oxygen 18 variations in the ocean and marine atmosphere.

Dansgaard, W. (1964). Stable isotopes in precipitation. *Tellus*, *16*(4), 436–468. https://doi.org/10.3402/tellusa.v16i4.8993

Diamond, R., Sime, L. C., Holmes, C. R., & Schroeder, D. (2024). CMIP6 models rarely simulate Antarctic winter sea-ice anomalies as large as observed in 2023. *Geophysical Research Letters*, *51*(10), e2024GL109265. https://doi.org/10.1029/2024GL109265

Dietrich, L. J., Steen-Larsen, H. C., Wahl, S., Jones, T. R., Town, M. S., & Werner, M. (2023). Snow-atmosphere humidity exchange at the ice sheet surface alters annual mean climate signals in ice core records. *Geophysical Research Letters*, *50*(20), e2023GL104249. https://doi.org/10.1029/2023GL104249

Dreossi, G., Masiol, M., Stenni, B., Zannoni, D., Scarchilli, C., Ciardini, V., et al. (2023). A decade (2008–2017) of water stable-isotope composition of precipitation at Concordia Station, East Antarctica. *EGUsphere*, *2023*, 1–38. https://doi.org/10.5194/egusphere-2023-2813

Dütsch, M., Blossey, P. N., Steig, E. J., & Nusbaumer, J. M. (2019). Nonequilibrium fractionation during ice cloud formation in iCAM5: Evaluating the common parameterization of supersaturation as a linear function of temperature. *Journal of Advances in Modeling Earth Systems*, *11*(11), 3777–3793. https://doi.org/10.1029/2019MS001764

Dütsch, M., Pfahl, S., & Sodemann, H. (2017). The impact of nonequilibrium and equilibrium fractionation on two different deuterium excess definitions. *Journal of Geophysical Research: Atmospheres*, *122*(23), 12732–12746. https://doi.org/10.1002/2017JD027085

EPICA community members. (2004). Eight glacial cycles from an Antarctic ice core. *Nature*, *429*(6992), 623–628. https://doi.org/10.1038/nature02599

Fiorella, R. P., Siler, N., Nusbaumer, J., & Noone, D. C. (2021). Enhancing understanding of the hydrological cycle via pairing of process-oriented and isotope ratio tracers. *Journal of Advances in Modeling Earth Systems*, *13*(10), e2021MS002648. https://doi.org/10.1029/2021MS002648

Gao, Q., Sime, L. C., McLaren, A. J., Bracegirdle, T. J., Capron, E., Rhodes, R. H., et al. (2024). Evaporative controls on Antarctic precipitation: An ECHAM6 model study using innovative water tracer diagnostics. *The Cryosphere*, *18*(2), 683–703. https://doi.org/10.5194/TC-18-683-2024

Gao, Q., Sime, L. C., McLaren, A. J., & Werner, M. (2025). Datasets for the article "Moisture source controls on water isotopes in Antarctic precipitation - Insights from water tracers in ECHAM6-wiso" [Dataset]. *Zenodo*. https://doi.org/10.5281/zenodo.15107251

Gorodetskaya, I. V., Durán-Alarcón, C., González-Herrero, S., Clem, K. R., Zou, X., Rowe, P., et al. (2023). Record-high Antarctic Peninsula temperatures and surface melt in February 2022: A compound event with an intense atmospheric river. *npj Climate and Atmospheric Science*, *6*(1), 1–18. https://doi.org/10.1038/s41612-023-00529-6

Hahn, L. C., Armour, K. C., Zelinka, M. D., Bitz, C. M., & Donohoe, A. (2021). Contributions to polar amplification in CMIP5 and CMIP6 models. *Frontiers in Earth Science*, *9*, 725. https://doi.org/10.3389/FEART.2021.710036/BIBTEX

Hersbach, H., Bell, B., Berrisford, P., Hirahara, S., Horányi, A., Muñoz-Sabater, J., et al. (2020). The ERA5 global reanalysis. *Quarterly Journal of the Royal Meteorological Society*, *146*(730), 1999–2049. https://doi.org/10.1002/qj.3803

Hoffmann, G., Werner, M., & Heimann, M. (1998). Water isotope module of the ECHAM atmospheric general circulation model: A study on timescales from days to several years. *Journal of Geophysical Research*, *103*(D14), 16871–16896. https://doi.org/10.1029/98JD00423

IPCC. (2021). *Climate change 2021: The physical science basis. Contribution of working group I to the sixth assessment report of the inter-governmental panel on climate change*. Cambridge University Press. In Press. https://doi.org/10.1017/9781009157896

Jouzel, J. (2014). Water stable isotopes: Atmospheric composition and applications in polar ice core studies. In *Treatise on geochemistry* (2nd ed., Vol. 5, pp. 213–256). Elsevier. https://doi.org/10.1016/B978-0-08-095975-7.00408-3

Jouzel, J., Delaygue, G., Landais, A., Masson-Delmotte, V., Risi, C., & Vimeux, F. (2013). Water isotopes as tools to document oceanic sources of precipitation. *Water Resources Research*, *49*(11), 7469–7486. https://doi.org/10.1002/2013WR013508

Jouzel, J., Masson-Delmotte, V., Cattani, O., Dreyfus, G., Falourd, S., Hoffmann, G., et al. (2007). Orbital and millennial Antarctic climate variability over the past 800,000 years. *Science*, *317*(5839), 793–796. https://doi.org/10.1126/science.1141038

Jouzel, J., & Merlivat, L. (1984). Deuterium and oxygen 18 in precipitation: Modeling of the isotopic effects during snow formation. *Journal of Geophysical Research*, *89*(D7), 11749–11757. https://doi.org/10.1029/JD089ID07P11749

Jouzel, J., Merlivat, L., & Lorius, C. (1982). Deuterium excess in an East Antarctic ice core suggests higher relative humidity at the oceanic surface during the last glacial maximum. *Nature*, *299*(5885), 688–691. https://doi.org/10.1038/299688a0

Jouzel, J., Vimeux, F., Caillon, N., Delaygue, G., Hoffmann, G., Masson-Delmotte, V., & Parrenin, F. (2003). Magnitude of isotope/temperature scaling for interpretation of central Antarctic ice cores. *Journal of Geophysical Research*, *108*(D12), 4361. https://doi.org/10.1029/2002JD002677

Kim, S. (2015). PPCOR: An R package for a fast calculation to semi-partial correlation coefficients. *Communications for Statistical Applications and Methods*, *22*(6), 665–674. https://doi.org/10.5351/CSAM.2015.22.6.665

Kurita, N., Hirasawa, N., Koga, S., Matsushita, J., Steen-Larsen, H. C., Masson-Delmotte, V., & Fujiyoshi, Y. (2016). Influence of large-scale atmospheric circulation on marine air intrusion toward the East Antarctic coast. *Geophysical Research Letters*, *43*(17), 9298–9305. https://doi.org/10.1002/2016GL070246

Landais, A., Stenni, B., Masson-Delmotte, V., Jouzel, J., Cauquoin, A., Fourré, E., et al. (2021). Interglacial Antarctic–Southern Ocean climate decoupling due to moisture source area shifts. *Nature Geoscience*, *14*(12), 918–923. https://doi.org/10.1038/s41561-021-00856-4

LeGrande, A. N., & Schmidt, G. A. (2006). Global gridded data set of the oxygen isotopic composition in seawater. *Geophysical Research Letters*, *33*(12), 12604. https://doi.org/10.1029/2006GL026011

Lenton, T. M., Rockström, J., Gaffney, O., Rahmstorf, S., Richardson, K., Steffen, W., & Schellnhuber, H. J. (2019). Climate tipping points—Too risky to bet against. *Nature*, *575*(7784), 592–595. https://doi.org/10.1038/d41586-019-03595-0

Lever, J., Krzywinski, M., & Altman, N. (2016). Model selection and overfitting. *Nature Methods*, *13*(9), 703–704. https://doi.org/10.1038/nmeth.3968

Majoube, M. (1971a). Fractionnement en 180 entre la glace et la vapeur d'eau. *Journal de Chimie Physique*, *68*, 625–636. https://doi.org/10.1051/JCP/1971680625

Majoube, M. (1971b). Fractionnement en oxygène 18 et en deutérium entre l'eau et sa vapeur. *Journal de Chimie Physique*, *68*, 1423–1436. https://doi.org/10.1051/JCP/1971681423

Markle, B. R., & Steig, E. J. (2022). Improving temperature reconstructions from ice-core water-isotope records. *Climate of the Past*, *18*(6), 1321–1368. https://doi.org/10.5194/CP-18-1321-2022

Masson-Delmotte, V., Hou, S., Ekaykin, A., Jouzel, J., Aristarain, A., Bernardo, R. T., et al. (2008). A review of antarctic surface snow isotopic composition: Observations, atmospheric circulation, and isotopic modeling. *Journal of Climate*, *21*(13), 3359–3387. https://doi.org/10.1175/2007JCLI2139.1

Merlivat, L. (1978). Molecular diffusivities of $H_2{}^{16}O$, $HD^{16}O$, and $H_2{}^{18}O$ in gases. *The Journal of Chemical Physics*, *69*(6), 2864–2871. https://doi.org/10.1063/1.436884

Merlivat, L., & Jouzel, J. (1979). Global climatic interpretation of the deuterium-oxygen 18 relationship for precipitation. *Journal of Geophysical Research*, *84*(C8), 5029–5033. https://doi.org/10.1029/JC084IC08P05029

Merlivat, L., & Nief, G. (1967). Fractionnement isotopique lors des changements d'état solide-vapeur et liquide-vapeur de l'eau à des températures inférieures à 0°C. *Tellus*, *19*(1), 122–127. https://doi.org/10.1111/J.2153-3490.1967.TB01465.X

Mottram, R., Hansen, N., Kittel, C., Van Wessem, J. M., Agosta, C., Amory, C., et al. (2021). What is the surface mass balance of Antarctica? An intercomparison of regional climate model estimates. *The Cryosphere*, *15*(8), 3751–3784. https://doi.org/10.5194/TC-15-3751-2021

Ollivier, I., Steen-Larsen, H. C., Stenni, B., Arnaud, L., Casado, M., Cauquoin, A., et al. (2024). Surface processes and drivers of the snow water stable isotopic composition at Dome C, East Antarctica – A multi-datasets and modelling analysis. *EGUsphere*, *2024*, 1–39. https://doi.org/10.5194/egusphere-2024-685

Palerme, C., Genthon, C., Claud, C., Kay, J. E., Wood, N. B., & L'Ecuyer, T. (2017). Evaluation of current and projected Antarctic precipitation in CMIP5 models. *Climate Dynamics*, *48*(1–2), 225–239. https://doi.org/10.1007/S00382-016-3071-1/TABLES/2

Pang, H., Hou, S., Landais, A., Masson-Delmotte, V., Jouzel, J., Steen-Larsen, H. C., et al. (2019). Influence of summer sublimation on δD, $\delta^{18}O$, and $\delta^{17}O$ in precipitation, east Antarctica, and implications for climate reconstruction from ice cores. *Journal of Geophysical Research: Atmospheres*, *124*(13), 7339–7358. https://doi.org/10.1029/2018JD030218

Pfahl, S., & Sodemann, H. (2014). What controls deuterium excess in global precipitation? *Climate of the Past*, *10*(2), 771–781. https://doi.org/10.5194/CP-10-771-2014

Pfahl, S., & Wernli, H. (2008). Air parcel trajectory analysis of stable isotopes in water vapor in the eastern Mediterranean. *Journal of Geophysical Research*, *113*(D20), 20104. https://doi.org/10.1029/2008JD009839

Purich, A., & Doddridge, E. W. (2023). Record low Antarctic sea ice coverage indicates a new sea ice state. *Communications Earth & Environment*, *4*(1), 1–9. https://doi.org/10.1038/s43247-023-00961-9

Risi, C., Bony, S., & Vimeux, F. (2008). Influence of convective processes on the isotopic composition ($\delta^{18}O$ and δD) of precipitation and water vapor in the tropics: 2. Physical interpretation of the amount effect. *Journal of Geophysical Research*, *113*(D19), 19306. https://doi.org/10.1029/2008JD009943

Risi, C., Bony, S., Vimeux, F., & Jouzel, J. (2010). Water-stable isotopes in the LMDZ4 general circulation model: Model evaluation for present-day and past climates and applications to climatic interpretations of tropical isotopic records. *Journal of Geophysical Research*, *115*(D12), 12118. https://doi.org/10.1029/2009JD013255

Risi, C., Landais, A., Winkler, R., & Vimeux, F. (2013). Can we determine what controls the spatio-temporal distribution of d-excess and ^{17}O-excess in precipitation using the LMDZ general circulation model? *Climate of the Past*, *9*(5), 2173–2193. https://doi.org/10.5194/CP-9-2173-2013

Ritter, F., Christian Steen-Larsen, H., Werner, M., Masson-Delmotte, V., Orsi, A., Behrens, M., et al. (2016). Isotopic exchange on the diurnal scale between near-surface snow and lower atmospheric water vapor at Kohnen station, East Antarctica. *The Cryosphere*, *10*(4), 1647–1663. https://doi.org/10.5194/TC-10-1647-2016

Sodemann, H., & Stohl, A. (2009). Asymmetries in the moisture origin of Antarctic precipitation. *Geophysical Research Letters*, *36*(22), L22803. https://doi.org/10.1029/2009GL040242

Sodemann, H., Weng, Y., Touzeau, A., Jeansson, E., Thurnherr, I., Barrell, C., et al. (2024). The cumulative effect of wintertime weather systems on the ocean mixed-layer stable isotope composition in the Iceland and Greenland seas. *Journal of Geophysical Research: Atmospheres*, *129*(19), e2024JD041138. https://doi.org/10.1029/2024JD041138

Steen-Larsen, H. C., Masson-Delmotte, V., Hirabayashi, M., Winkler, R., Satow, K., Prié, F., et al. (2014). What controls the isotopic composition of Greenland surface snow? *Climate of the Past*, *10*(1), 377–392. https://doi.org/10.5194/CP-10-377-2014

Steen-Larsen, H. C., Risi, C., Werner, M., Yoshimura, K., & Masson-Delmotte, V. (2017). Evaluating the skills of isotope-enabled general circulation models against in situ atmospheric water vapor isotope observations. *Journal of Geophysical Research: Atmospheres*, *122*(1), 246–263. https://doi.org/10.1002/2016JD025443

Stenni, B., Masson-Delmotte, V., Selmo, E., Oerter, H., Meyer, H., Röthlisberger, R., et al. (2010). The deuterium excess records of EPICA Dome C and Dronning Maud Land ice cores (East Antarctica). *Quaternary Science Reviews*, *29*(1–2), 146–159. https://doi.org/10.1016/J.QUASCIREV.2009.10.009

Stenni, B., Scarchilli, C., Masson-Delmotte, V., Schlosser, E., Ciardini, V., Dreossi, G., et al. (2016). Three-year monitoring of stable isotopes of precipitation at Concordia Station, East Antarctica. *The Cryosphere*, *10*(5), 2415–2428. https://doi.org/10.5194/TC-10-2415-2016

Stevens, B., Giorgetta, M., Esch, M., Mauritsen, T., Crueger, T., Rast, S., et al. (2013). Atmospheric component of the MPI-M Earth system model: ECHAM6. *Journal of Advances in Modeling Earth Systems*, *5*(2), 146–172. https://doi.org/10.1002/JAME.20015

Thurnherr, I., Kozachek, A., Graf, P., Weng, Y., Bolshiyanov, D., Landwehr, S., et al. (2020). Meridional and vertical variations of the water vapour isotopic composition in the marine boundary layer over the Atlantic and Southern Ocean. *Atmospheric Chemistry and Physics*, *20*(9), 5811–5835. https://doi.org/10.5194/ACP-20-5811-2020

Uemura, R., Masson-Delmotte, V., Jouzel, J., Landais, A., Motoyama, H., & Stenni, B. (2012). Ranges of moisture-source temperature estimated from Antarctic ice cores stable isotope records over glacial-interglacial cycles. *Climate of the Past*, *8*(3), 1109–1125. https://doi.org/10.5194/CP-8-1109-2012

Uemura, R., Matsui, Y., Yoshimura, K., Motoyama, H., & Yoshida, N. (2008). Evidence of deuterium excess in water vapor as an indicator of ocean surface conditions. *Journal of Geophysical Research*, *113*(D19), 19114. https://doi.org/10.1029/2008JD010209

Vimeux, F., Masson, V., Jouzel, J., Petit, J. R., Steig, E. J., Stievenard, M., et al. (2001). Holocene hydrological cycle changes in the Southern Hemisphere documented in East Antarctic deuterium excess records. *Climate Dynamics*, *17*(7), 503–513. https://doi.org/10.1007/PL00007928/METRICS

Wahl, S., Steen-Larsen, H. C., Reuder, J., & Hörhold, M. (2021). Quantifying the stable water isotopologue exchange between the snow surface and lower atmosphere by direct flux measurements. *Journal of Geophysical Research: Atmospheres*, *126*(13), e2020JD034400. https://doi.org/10.1029/2020JD034400

Werner, M., Heimann, M., & Hoffmann, G. (2001). Isotopic composition and origin of polar precipitation in present and glacial climate simulations. *Tellus B: Chemical and Physical Meteorology*, *53*(1), 53–71. https://doi.org/10.3402/TELLUSB.V53I1.16539

Zannoni, D., Steen-Larsen, H. C., Peters, A. J., Wahl, S., Sodemann, H., & Sveinbjörnsdóttir, A. E. (2022). Non-equilibrium fractionation factors for D/H and $^{18}O/^{16}O$ during oceanic evaporation in the North-West Atlantic Region. *Journal of Geophysical Research: Atmospheres*, *127*(21), e2022JD037076. https://doi.org/10.1029/2022JD037076